Electronic Supplementary Material (ESI) for Materials Chemistry Frontiers.

Supplementary Information

Mo-triggered Amorphous Ni_3S_2 Nanosheets as Efficient and Durable Electrocatalysts for Water Splitting

Haoxuan Zhang,[a] Hao Jiang,*[a] Yanjie Hu,[a] Petr Saha,[b] Chunzhong Li*[a]

[a] Key Laboratory for Ultrafine Materials of Ministry of Education & School of Materials Science and Engineering, East China University of Science and Technology, Shanghai 200237, China

[b] Centre of Polymer Systems, University Institute, Tomas Bata University in Zlin, Trida T. Bati 5678, 760 01 Zlin, Czech Republic

Email: jianghao@ecust.edu.cn (Prof. H. Jiang) and czli@ecust.edu.cn (Prof. C. Z. Li)

Part I: Experimental Section

1.1 Synthesis of a-Mo-Ni_3S_2 nanosheets:

Prior to use, commercial Ni foam (0.6 cm × 0.5 cm × 0.3 mm) was immersed in 3 M HCl for 20 minutes to remove surface oxide layer. In a typical synthesis, 8 mmol of CH_3CSNH_2 and 2 mmol of Na_2MoO_4 were grinded in a mortar for 10 minutes. The mixture was then put into a 5 mL flask. Subsequently, a piece of cleaned Ni foam was embedded in the mixture at 220 ˚C for 40 minutes. After cooled down to room temperature, washed with distilled water, absolute ethanol and carbon disulfide for several times, the resulting products have been obtained. The Mo content in products can be easily controlled by changing the amount of Na_2MoO_4, *e.g.* 6.3 % (0.5 mmol), 7.4 % (1.0 mmol), 11.5 % (1.5 mmol), 12.5 % (2.0 mmol) and 16.7 (2.5 mmol). Without the addition of Na_2MoO_4, the crystalline Ni_3S_2 products have been obtained.

1.2 Characterization:

Scanning electron microscopy (SEM) images were taken from a Hitachi, S-4800 FE-SEM at an accelerating voltage of 15.0 kV. Transmission electron microscopy (TEM) and high-resolution transmission (HR-TEM) images were taken from a JEOL, JEM-2100F TEM with an X-ray Energy-dispersive spectrometer (EDS) at an accelerating voltage of 200.0 kV. X-ray powder diffraction (XRD) patterns were recorded on a Rigaku D/Max 2550 diffractometer with Cu Kα radiation at a scan rate of 1° min^{-1}. X-ray photoelectron spectroscopy (XPS) spectra were recorded on an ESCALAB 250Xi X-ray photoelectron spectrometer at a pass energy of 40 eV with an Al Kα X-ray source. Inductively coupled plasma mass spectrometry (ICP-MS) was performed by an Agilient 7700 spectrometer. The samples were directly conducted by X-ray diffraction and scanning electron microscopy, and were dispersed in absolute ethanol for 10-min ultrasound bath before transmission electron microscopy, and were grinded to powder for X-ray photoelectron spectra and inductively coupled plasma mass spectrometry.

1.3 Electrochemical Measurements:

The electrochemical measurements for HER and OER were performed in a standard three-electrode system controlled by a CHI660E electrochemical workstation (Chenhua, Shanghai) with saturated Ag/AgCl and graphite electrode as reference electrode and counter electrode, respectively. The electrocatalysts supported on Ni foam were directly used as working electrode. All measurements were carried out in 1.0 M KOH aqueous solution under gently stirring to remove bubbles. The measured potentials were calibrated to reversible hydrogen electrode (RHE) by the following equation:

$$E_{RHE} = E_{Ag/Agcl} + 0.1976 + 0.0591 \times pH$$

Before HER and OER tests, the electrolyte was purged with N_2 and O_2 for at least 30 minutes to achieve an N_2 and O_2-saturated condition, respectively. After that, the electrocatalysts were activated at a constant current density of 10 mA cm^{-2} until attaining stable potentials. The LSV curves were recorded at a scan rate of 1 mV s^{-1}. The chronopotentiometry was performed under the same condition. The electrochemical data was presented with 95% *iR* drop compensation. The solution resistance (R) was calculated based on the electrochemical impedance spectroscopy (EIS) results measured at -0.15 V *vs.* RHE for HER and 1.53 V *vs.* RHE for OER in frequencies range from 10 kHz to 100 mHz. The resistance value is equal to the total impedance at the phase angle of 0° in high frequency. The turnover frequency (TOF) was calculated by the following equation:

$$TOF = \frac{J \times A}{2 \times F \times \mathrm{n}}$$

where J is the current density in the LSV curves, A is the geometric area of electrode, F is the Faraday constant (C mol^{-1}), and n is the mole number of active sites on the electrode.

Part II: Supporting Figures

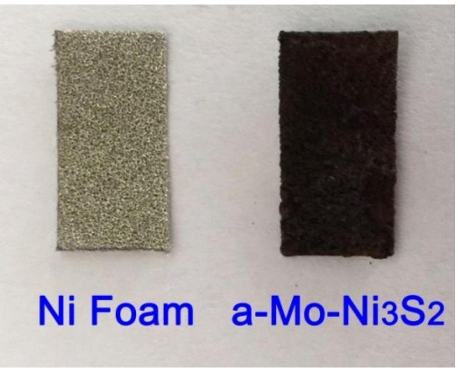

Fig. S1 Digital photograph of pristine Ni foam and the a-Mo-Ni_3S_2 nanosheets.

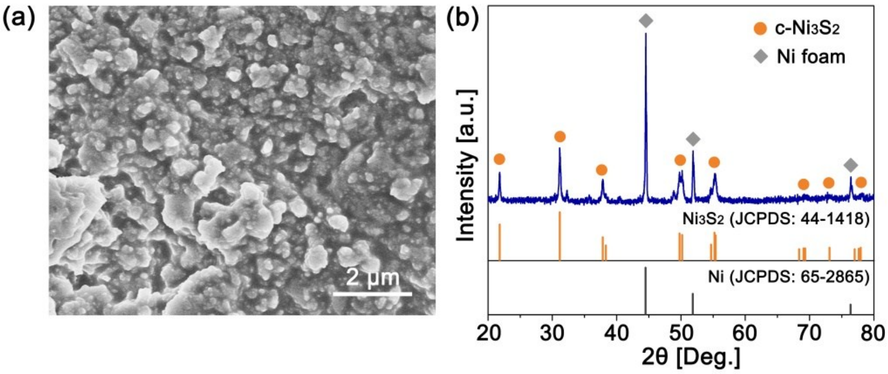

Fig. S2 (a) SEM image and (b) XRD pattern of the c-Ni_3S_2 products.

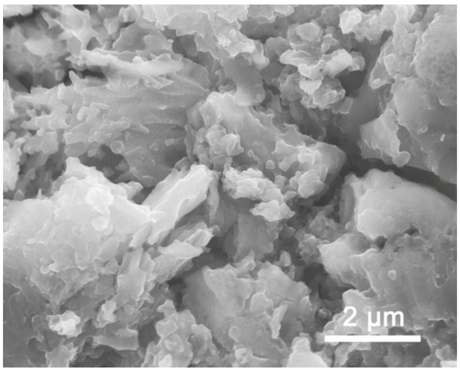

Fig. S3 SEM image of the a-Mo-Ni_3S_2 nanosheets.

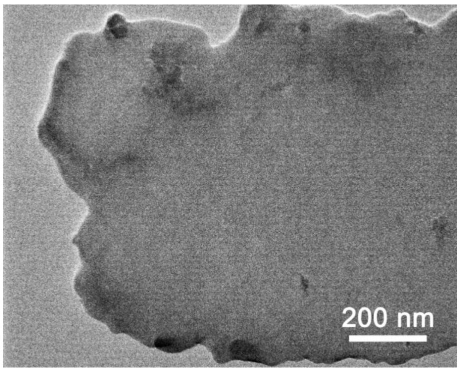

Fig. S4 TEM image of the a-Mo-Ni_3S_2 nanosheets.

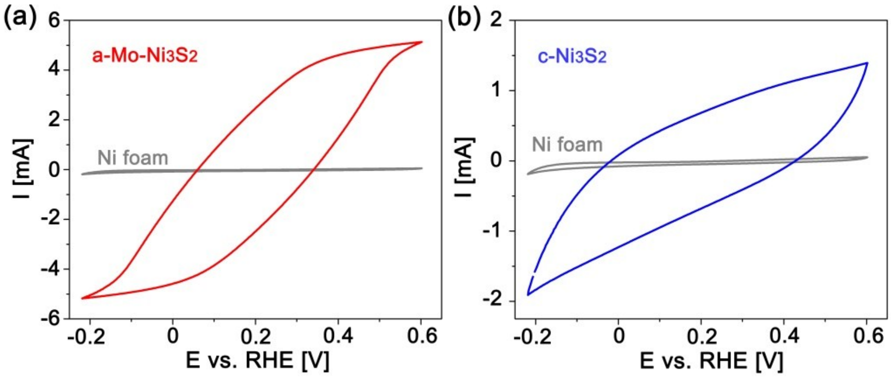

Fig. S5 Cyclic voltammograms curves of (a) the a-Mo-Ni_3S_2 and (b) the c-Ni_3S_2 electrocatalysts with pristine Ni foam as a control in pH = 7 at a scan rate of 50 mV s^{-1}.

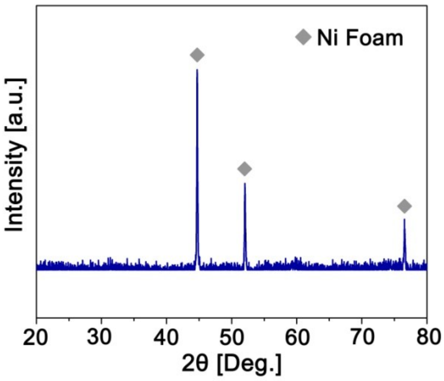

Fig. S6 XRD pattern of the a-Mo-Ni_3S_2 electrocatalysts after HER.

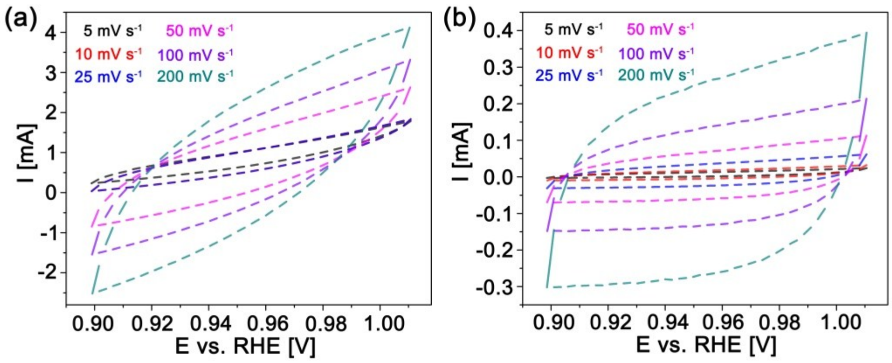

Fig. S7 Cyclic voltammograms curves of (a) the a-Mo-Ni_3S_2 and (b) the c-Ni_3S_2 electrocatalysts in the non-faradic potential range of 0.9 - 1.0 V at different scan rates.

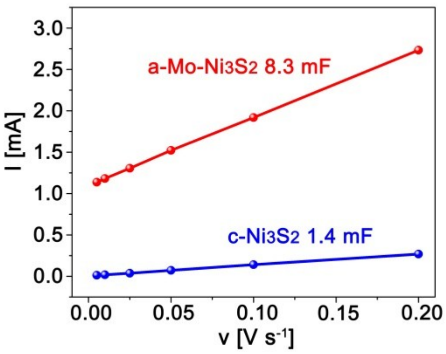

Fig. S8 The charging currents measured at 0.95 V *vs.* RHE plotted as a function of scan rate. The double-layer capacitance of the a-Mo-Ni_3S_2 and the c-Ni_3S_2 electrocatalysts is obtained from the slope of the linear fits to the data.

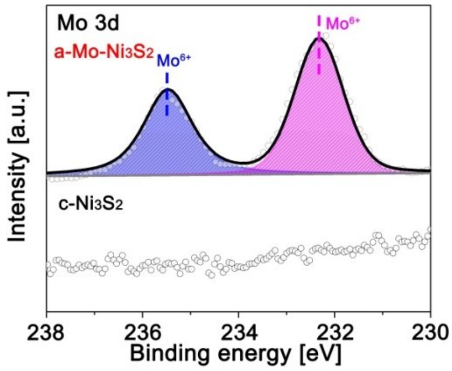

Fig. S9 Mo 3d XPS spectra of the a-Mo-Ni_3S_2 and the c-Ni_3S_2 electrocatalysts after HER.

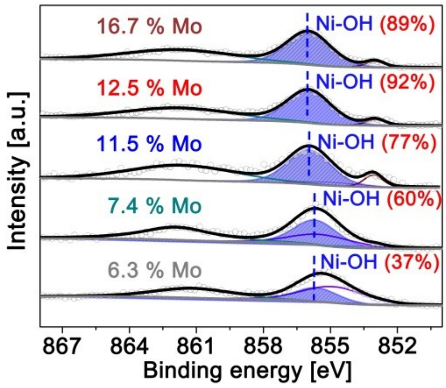

Fig. S10 Ni $2p_{3/2}$ XPS spectra of the Mo-Ni_3S_2 products with different Mo content after HER.

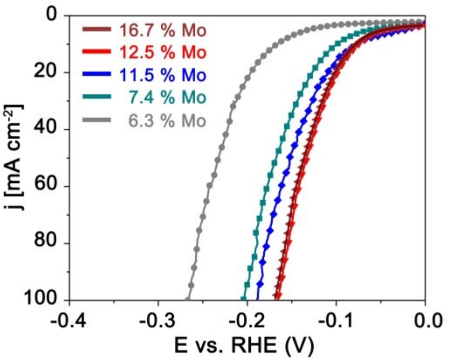

Fig. S11 HER polarization curves of the Mo-doped Ni_3S_2 products with different Mo content.

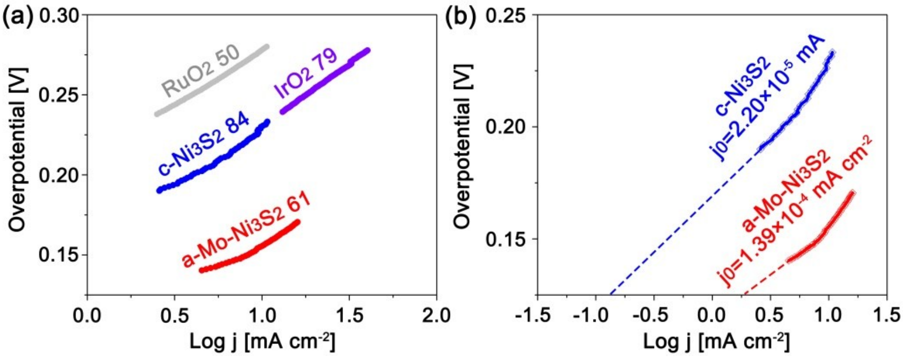

Fig. S12 (a) Tafel plots of the a-Mo-Ni_3S_2, the c-Ni_3S_2, the commercial IrO_2 and RuO_2 electrocatalysts, (b) the calculated exchange current density of the a-Mo-Ni_3S_2 and c-Ni_3S_2 electrocatalysts for OER. Such excellent OER performances of a-Mo-Ni_3S_2 catalysts surpass other reported electrocatalysts to date. For instance, Zou et al. reported amorphous Ni-Fe bimetallic hydroxide film-coated, nickel foam-supported, Ni_3S_2 nanosheet arrays by a facile ultrafast synthetic approach, which required a higher overpotential of 320 mV to obtain 100 mA cm^{-2}.[S1]

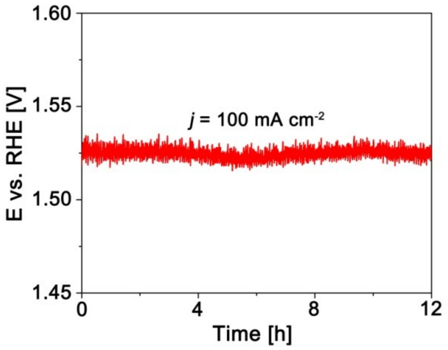

Fig. S13 Chronopotentiometry curve of the a-Mo-Ni_3S_2 electrocatalysts for OER.

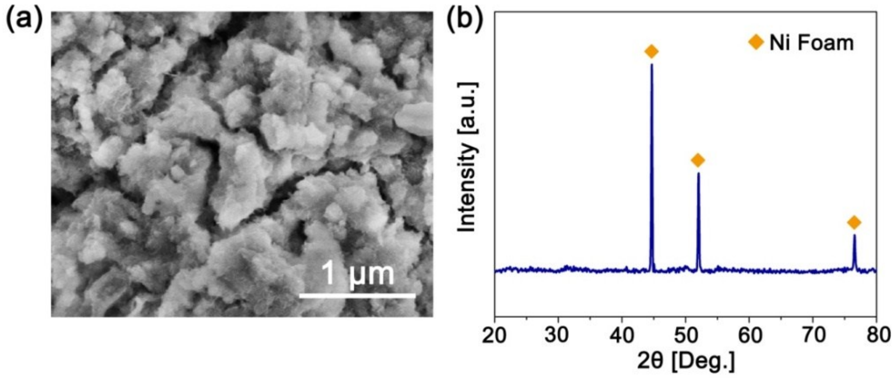

Fig. S14 (a) SEM image and (b) XRD pattern of the a-Mo-Ni_3S_2 electrocatalysts after OER.

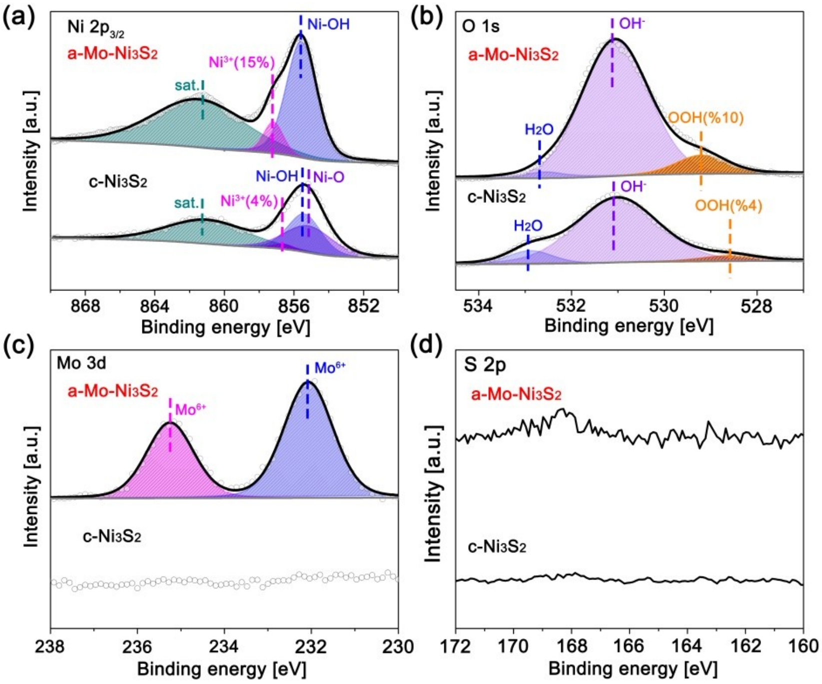

Fig. S15 XPS spectra of (a) Ni $2p_{3/2}$, (b) O 1s, (c) Mo 3d and (d) S 2p regions of the a-Mo-Ni_3S_2 and the c-Ni_3S_2 electrocatalysts after OER. For Ni $2p_{3/2}$ region, the peak at 857.2 eV in the a-Mo-Ni_3S_2 samples indicates the Ni^{3+} generation during OER. The Ni^{3+} content is 15 % by integrating the respective peak areas, nearly four times higher than the c-Ni_3S_2. For O 1s region, the peak of OOH* intermediates appears at 529.1 eV in the a-Mo-Ni_3S_2 with the content of 10 %, which is two times higher than the c-Ni_3S_2.

Part III: Supporting Table

Tab. S1 The comparisons of HER performance of various Ni-based electrocatalysts.

Electrocatalyst	Measurement	J (mA cm^{-2})	η (mV)	Tafel slope (mV dec^{-1})	Reference
Cu@CoS$_x$	Cu foam 1.0 M KOH	10	134	61	8
MoO$_x$/Ni$_3$S$_2$ microsphere	Ni foam 1.0 M KOH	10	106	90	11
Ni$_3$S$_2$ nanosheet arrays	Ni foam 1.0 M KOH	10	223	/	12
N doped Ni$_3$S$_2$ nanosheets	Ni foam 1.0 M KOH	10	155	113	S2
Cu decorated Ni$_3$S$_2$ nanotubes	Carbon fiber 1.0 M KOH	10	128	76	S3
Ni(OH)$_2$@CuS	Glass carbon 1.0 M KOH	10	95	104	S4
NiCu@C	Graphite plate 1.0 M KOH	10	74	94	S5
MoS$_2$-Ni$_3$S$_2$ heteronanorods	Ni foam 1.0 M KOH	10 100	98 191	61	S6
Ni$_x$Co$_{3-x}$S$_4$/Ni$_3$S$_2$ nanosheet arrays	Ni foam 1.0 M KOH	10	136	107	S7
Ni(OH)$_2$ nanosheets	Carbon cloth 1.0 M KOH	10	80	70	S8
Fe-doped Ni$_3$S$_2$ nanosheets	Ni foam 1.0 M KOH	50	214	/	S9
V-doped NiS$_2$ nanosheets	Glass carbon 1.0 M KOH	10	110	90	S10
N decorated Ni$_3$S$_2$	Ni foam 1.0 M KOH	10	110	70	S11
Ni/NiP	Ni foam 1.0 M KOH	10	130	58	S12
Porous Ni$_2$P	Ni foam 1.0 M KOH	10	98	72	S13
MoS$_2$-Ni$_3$S$_2$ heterostructures	Ni foam 1.0 M KOH	10	110	83	S14
Ni-P nanosheets	Carbon cloth 1.0 M KOH	10	98	59	S15
This work	**Ni foam 1.0 M KOH**	**10 50 100**	**74 134 165**	**54**	

References

S1 X. Zou, Y. Liu, G. D. Li, Y. Wu, D. P. Liu, W. Li, H. W. Li, D. Wang, Y. Zhang, X. Zou, *Adv. Mater.* 2017, **29**, 1700404

S2 T. Kou, T. Smart, B. Yao, I. Chen, D. Thota, Y. Ping, Y. Li, *Adv. Energy Mater.* 2018, 1703538.

S3 J. X. Feng, J. Q. Wu, Y. X. Tong, G. R. Li, *J. Am. Chem. Soc.* 2018, **140**, 610.

S4 S. Q. Liu, H. R. Wen, G. Ying, Y. W. Zhu, X. Z. Fu, R. Sun, C. P. Wong, *Nano Energy* 2018, **44**, 7.

S5 Y. Shen, Y. Zhou, D. Wang, X. Wu, J. Li, J. Xi, *Adv. Energy Mater.* 2017, **8**, 1701759.

S6 Y. Yang, K. Zhang, H. Lin, X. Li, H. C. Chan, L. Yang, Q. Gao, *ACS Catal.* 2017, **7**, 2357.

S7 Y. Wu, Y. Liu, G. D. Li, X. Zou, X. Lian, D. Wang, L. Sun, T. Asefa, X. Zou, *Nano Energy* 2017, **35**, 161.

S8 C. Hu, Q. Ma, S. F. Hung, Z. N. Chen, D. Ou, B. Ren, H. M. Chen, G. Fu, N. Zheng, *Chem* 2017, **3**, 122.

S9 Y. J. Li, H. C. Zhang, M. Jiang, Q. Zhang, P. L. He, X. M. Sun, *Adv. Funct. Mater.* 2017, **27**, 1702513.

S10 H. Liu, Q. He, H. Jiang, Y. Lin, Y. Zhang, M. Habib, S. Chen, L. Song, *ACS Nano* 2017, **11**, 11574.

S11 P. Chen, T. Zhou, M. Zhang, Y. Tong, C. Zhong, N. Zhang, L. Zhang, C. Wu, Y. Xie, *Adv. Mater.* 2017, **29**, 1701584.

S12 G. F. Chen, T. Y. Ma, Z. Q. Liu, N. Li, Y. Z. Su, K. Davey, S. Z. Qiao, *Adv. Funct.*

Mater. 2016, **26**, 3314.

S13 B. You, N. Jiang, M. Sheng, M. W. Bhushan, Y. Sun, *ACS Catal.* 2016, **6**, 714.

S14 J. Zhang, T. Wang, D. Pohl, B. Rellinghaus, R. Dong, S. Liu, X. Zhuang, X. Feng, *Angew. Chem. Int. Ed*. 2016, **55**, 6701.

S15 X. Wang, W. Li, D. Xiong, D. Y. Petrovykh, L. Liu, *Adv. Funct. Mater.* 2016, **26**, 4067.